Proceedings of 14th International Heat Transfer Conference
IHTC-14
August 8-13, 2010, Washington D.C., USA

IHTC14-22953

THE EFFECT OF INTERSTITIAL LAYERS ON THERMAL BOUNDARY CONDUCTANCE BETWEEN LENNARD-JONES CRYSTALS

Timothy S. English
Dept. of Mech. and Aero. Engr.
University of Virginia
Charlottesville, Virginia 22903
Email: tse8v@virginia.edu

John C. Duda
Dept. of Mech. and Aero. Engr.
University of Virginia
Charlottesville, Virginia 22903
Email: duda@virginia.edu

Donald A. Jordan
Dept. of Mech. and Aero. Engr.
University of Virginia
Charlottesville, Virginia 22903
Email: dojo@virginia.edu

Pamela M. Norris
Dept. of Mech. and Aero. Engr.
University of Virginia
Charlottesville, Virginia 22903
Email: pamela@virginia.edu

Leonid V. Zhigilei
Dept. of Mater. Sci. Engr.
University of Virginia
Charlottesville, Virginia 22903
Email: lz2n@virginia.edu

ABSTRACT

Thermal transport at the interface between Lennard-Jones crystals is explored via non-equilibrium molecular dynamics simulations. The vibrational properties of each crystal are varied by changing the atomic mass of the crystal. By applying a constant thermal flux across the two-crystal composite system, a steady-state temperature gradient is established and thermal boundary conductance at the interface between the crystals is calculated via Fourier's law. With the material properties of the two crystals fixed, thermal boundary conductance can be affected by an intermediate layer inserted between the two crystals. It is found that when the interstitial layer atomic mass is between those values of the crystals comprising the interface, interfacial transport is enhanced. This layer helps bridge the gap between the different vibrational spectra of the two materials, thus enhancing thermal transport, which is maximized when the interstitial layer atomic mass approaches the average mass of the two fixed crystals. The degree of enhancement depends on the vibrational mismatch between the interstitial layer and the crystals comprising the interface, and we report an increase in thermal boundary conductance of up to 50 %.

NOMENCLATURE

F force acting on an atom, [N]
h_{BD} thermal boundary conductance, [W m^{-2} K^{-1}]
h^*_{BD} reduced thermal boundary conductance
k thermal conductivity, [W m^{-1} K^{-1}]
k_{B} Boltzmann's Constant, [J K^{-1}]
m atomic mass, [kg]
q applied heat flux across the interface, [W m^{-2}]
R_{BD} thermal boundary resistance, [m^2 K W^{-1}]
t time, [s]
T temperature, [K]
T^* reduced temperature
U potential energy, [J]
v atomic velocity, [m s^{-1}]
ε Lennard-Jones parameter, [J]
σ Lennard-Jones parameter, [m]
ξ scaling factor implemented in NEMD
ω vibrational frequency, [Hz]
N_P number of atoms in a particular slice P

Subscripts
i, j atomic indices

INTRODUCTION

The continuing miniaturization of today's nano- and optoelectronic devices is introducing more interfaces per unit length for energy carriers, i.e., phonons or electrons, to traverse. As a result, the primary thermal resistance in many modern devices is the Kapitza or thermal boundary resistance (R_{BD}) at the various interfaces within these devices. In general, resistance to thermal flow in solids is due to the scattering of energy carriers as they propagate through the medium. The distance between these scattering events, described by the mean free path (MFP), is 10 to 100 nm at room temperature [1]. Abrupt interfaces provide yet another site for carrier scattering. In modern nanostructured devices, these interfaces are often spaced at distances smaller than the carrier MFP, thus scattering is dictated by interfaces between the materials and not the materials themselves. Consequently, R_{BD} is of ever-growing importance within the the nanoelectronics and photonics industries [2].

Thermal boundary resistance was first detected at the interface between a solid and superfluid helium by Kapitza [3]. This Kapitza resistance exists at solid-solid interfaces as well, and while smaller than that at the solid-liquid interface, it is of increasing importance as characteristic lengths continue to decrease. Due to the carrier scattering attributed to R_{BD} there is an abrupt finite temperature drop ΔT at an interface between dissimilar materials when a heat flux q is applied across the interface. This temperature drop is related to the magnitude of the flux and R_{BD} through the expression

$$q = \frac{1}{R_{\mathrm{BD}}}\Delta T = h_{\mathrm{BD}}\Delta T, \tag{1}$$

where h_{BD} is the thermal boundary conductance, or inverse of R_{BD}. Traditionally, h_{BD} has been seen as a property of the materials comprising the interface: the more vibrationally dissimilar the materials, the less conductive the interface [4–6]. However, while acoustic or vibrational properties often dictate the magnitude of h_{BD} at interfaces between highly dissimilar materials, the quality of the interface is important as well [7]. The effects of interfacial structure and defects on h_{BD} become more prominent as the relative vibrational mismatch between the materials, often summarized by the difference in Debye temperatures, becomes smaller. For example, Hopkins *et al.* [8] demonstrated that atomic mixing and the spatial extent of the mixing region at the interface between chromium and silicon have a significant effect on the magnitude of h_{BD}.

Investigating the effects of interfacial conditions on h_{BD} through experimental means can be difficult due to the lack of complete control during sample fabrication processes. On the contrary, molecular dynamics (MD) simulations are capable of quickly and systematically controlling the attributes of a material system atom by atom. This, in combination with the fact that MD can be used to evaluate the thermal properties of these nanoscale systems, i.e., thermal conductivity [9, 10], thermal expansion, laser induced melting and ablation of thin metallic films [11], and thermal boundary conductance [12–17], make MD simulations a powerful research tool for the investigation of thermal transport phenomena at the nanoscale.

Two different approaches exist for determining thermal properties of a system through the use of molecular dynamics: the equilibrium approach via the Green-Kubo (GK) method, and the direct method, otherwise known as non-equilibrium molecular dynamics (NEMD). The first approach examines the statistical fluctuations of thermal current about zero compared to the time between these fluctuations, relating thermal conductivity to the thermal current autocorrelation function through the Green-Kubo expression. The non-equilibrium method parallels the approach of a typical laboratory experiment. A temperature gradient is created across the computational domain by adding energy to one end of the domain (the hot bath) and removing the same amount of energy from the other end of the domain (the cold bath). Upon reaching steady-state, Fourier's law can be applied and thermal properties determined. While it has been shown that these two methods do not differ for homogeneous systems [18], it is not clear if the GK approach can be applied to heterogeneous systems. Due to the multi-component computational domains explored in this study, the NEMD approach was implemented.

Many previous studies have investigated h_{BD} via MD simulations [12–17]. Pickett *et al.* used the GK method to investigate energy transfer across diamond lattice systems that differ only in atomic mass, and hence, vibrational properties (that is, $\omega \propto m^{-1/2}$). Using the Stillinger-Weber (SW) potential to model the diamond-structure crystals (specifically, silicon), they found that seemingly small differences in atomic mass can have an impact on the vibrational coupling across the interface between the mass-mismatched crystals [12]. Maiti *et al.* report one of the earliest implementations of NEMD simulations, using it to investigate the effects of local disorder on h_{BD} at grain boundaries in silicon [13]. Twu and Ho examined the impact of interface imperfections, i.e., atomic mixing and the presence of vacancies, on the Kapitza resistance using the direct NEMD method [14]. They found that the Kapitza resistance increased with an increase in the degree of disorder at the interface. Stevens *et al.* investigated the effects of relative acoustic mismatch, lattice constant mismatch, and interfacial mixing on h_{BD} at interfaces in systems described by the Lennard-Jones (LJ) interatomic potential. They found that h_{BD} decreased with increasing acoustic mismatch, lattice constant mismatch had a larger impact for interfaces comprised of acoustically matched materials, and that controlled interfacial mixing improved transport by nearly a factor of two [15]. Lyver IV and Blaisten-Barojos also looked at h_{BD} between LJ crystals. The properties of the LJ crystals were systematically varied by changing either ε, σ, or m of the atoms comprising one of the crystals relative to the reference state [16].

Interfaces between symmetrically strained Si and Ge, as well as between Si and "heavy" Si, were studied both theoretically and through the use of NEMD by Landry and McGaughey [17].

In additional to the former studies, at least one group has looked more directly at the affect of a thin film on interfacial transport via LJ crystals. Hegedus and Abramson explored nanocomposite systems including an ultra-thin film layer composed of 8 planes of atoms [19]. In their simulations, the atomic mass, m, and LJ bond strength parameter, ε, were systematically varied between 25% and 200 % of their respective baseline values. However, the material properties of the crystals on each side of the thin film were identical. As a result, in the ideal case where the thin film layer properties are set equal to those of the surrounding system (100% of the baseline value), no interface or thermal resistance exists, resulting in a maximum in thermal conductivity. Furthermore, their study shows an inverse parabolic dependence between the effective thermal conductivity and the atomic mass of the thin film layer. The effective thermal conductivity across the computational domain decreases as the magnitude of the difference between the baseline mass and thin film mass increases.

In this study, a novel method to enhance interfacial thermal transport utilizing an interstitial layer is investigated using NEMD. Unlike the study performed by Hegedus and Abramson, in this study, the baseline system consists of an interface characterized by a large vibrational mismatch. While the interstitial layer is shown to broadly enhance thermal transport, the degree of enhancement depends directly on the vibrational (phonon) spectra of the interstitial layer, providing an avenue for tuning of the thermal properties at the interface.

Thermal boundary conductance is calculated for a system of two LJ crystals differing only in atomic mass to form a baseline reference value. With the material properties of the two crystals fixed, the effect of a third Lennard-Jones crystal, serving as an interstitial layer at the interface, is explored. The vibrational properties of the interstitial crystal are systematically varied by changing the atomic mass of the crystal. It is generally found that an interstitial layer will enhance the thermal conductance of an interface so long as it's vibrational properties fall between those of the two crystals comprising the interface. Additionally, our results indicate that the maximum in thermal boundary conductance occurs when the interstitial layer mass approaches the average mass of the two fixed crystals.

MOLECULAR DYNAMICS SIMULATIONS

The computational domain used in this study is an FCC crystal with a square cross section (equal dimensions along the x-axis and y-axis) oriented such that the [100] direction is extended along the z-axis. The domain was divided in half, where each half was occupied by atoms with a different atomic mass. Interactions between the atoms were described by the Lennard-Jones potential,

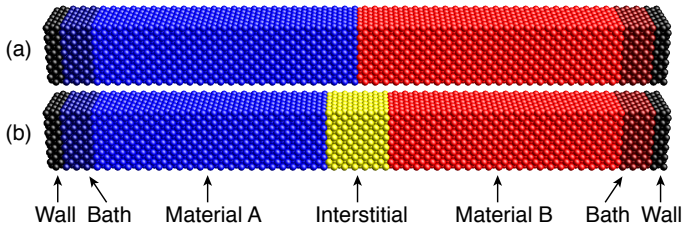

Figure 1. SCHEMATICS OF COMPUTATIONAL CELLS.

$$U_{\mathrm{LJ}}(r_{ij}) = 4\varepsilon\left[\left(\frac{\sigma}{r_{ij}}\right)^{12} - \left(\frac{\sigma}{r_{ij}}\right)^{6}\right]. \tag{2}$$

The potential parameters used in this study to describe the system were $\sigma = 3.37$ Å and $\varepsilon = 0.0503$ eV [20]. A representative schematic of the computational cell is shown in Fig. 1. Figure 1a represents the two-material computational cell used for determining a baseline value of h_{BD} for a perfect (sharp) interface, where blue spheres represent material A and red spheres represent material B. Figure 1b illustrates the three-material computational cell used to investigate the effects of an interstitial layer, where yellow atoms belong to the interstitial layer (material C).

During the simulation, the equations of motion for the system were integrated using the Nordsieck fifth-order predictor corrector algorithm. Periodic boundary conditions were initially applied in all directions and the system was equilibrated at a predefined temperature and zero pressure. The pressure was maintained by the Berendsen barostat algorithm [21]. Once equilibration was complete, boundary conditions in the z-direction were switched from periodic to free boundary conditions and the non-equilibrium heating procedure was implemented. The addition of energy to (or removal from) the baths at either end of the simulation cell was performed in a similar fashion to the procedure outlined by Ivanov and Zhigilei for energy exchange between electronic and lattice systems during simulations of short pulse laser heating of metals [11]. This routine slightly changes the forces acting on a particular atom depending on the amount of energy to be added or removed. The total force acting on atom i is given by

$$F_{i,\mathrm{total}} = F_i + \xi m_i v_i^T, \tag{3}$$

where m_i is the mass of the atom, v_i^T is the thermal velocity of the atom, and ξ is a scaling factor. This scaling factor is expressed as

$$\xi = q\frac{1}{2K^T} = \frac{\Delta E}{2\Delta t K^T}, \tag{4}$$

where Δt is the time step used in the MD integration of the equations of motion, ΔE is the amount of energy to be added to or removed from the bath per time step, and K^T is the total thermal kinetic energy of the bath. To ensure the baths were not being perturbed far from equilibrium they were sized such that the amount of energy added or removed from the bath was less than 1% of the bath kinetic energy. In all simulations, 6 atomic planes per bath were sufficient to satisfy this constraint. This constant-energy approach was preferred over maintaining the baths at a specific temperature because applied flux was exactly known and not subject to statistical fluctuations, as is the case when baths are maintained at constant temperatures. In order to prevent evaporation of the bath atoms, rigid walls were added to the outside edge of each bath.

During non-equilibrium heating, the system was divided into 40 equally sized slices such that a spatial temperature profile could be calculated along the z-axis. The temperature of each of these slices was determined through the following relationship

$$\frac{3}{2}N_P k_B T_P = \sum_{i=1}^{N_P} \frac{1}{2} m_i \left(v_i^T\right)^2, \tag{5}$$

where N_P is the number of atoms in a particular slice P, and k_B is Boltzmann's constant. Each slice is comprised of approximately 216 atoms. Linear least-squares fits of temperature versus time data were made for discrete time intervals during the simulation and the slopes of these lines were used to monitor the establishment of the steady-state regime. In all cases, the slopes converged to values oscillating around zero (on the order of +/- 0.02), which can be attributed to a statistical noise component introduced as the simulation iterates over each time step. As an example, the temperatures of selected slices versus time are shown in Figure 2, illustrating the initial heating and cooling as well as the transition to the steady-state regime. In this and all subsequent discussions, temperature and thermal boundary conductance values are presented in reduced Lennard-Jones units in order to simplify the comparison of results, and are expressed using the following equations,

$$T^* = T\frac{k_B}{\varepsilon},\ h^*_{BD} = h_{BD} * \frac{m^{0.5}\sigma^3}{\varepsilon^3 k_B} \tag{6}$$

Once in the steady-state regime, time-averaged temperature profiles were created, an example of which is shown in Figure 3. A linear least-squares fit was performed for each half of the temperature profile to calculate the slope of the temperature gradient. The two atomic planes closest to the edge of the simulation cell and the interface were not included in the fits. The temperature drop at the interface was determined by extrapolating each linear fit to the geometric center of the simulation cell. From the

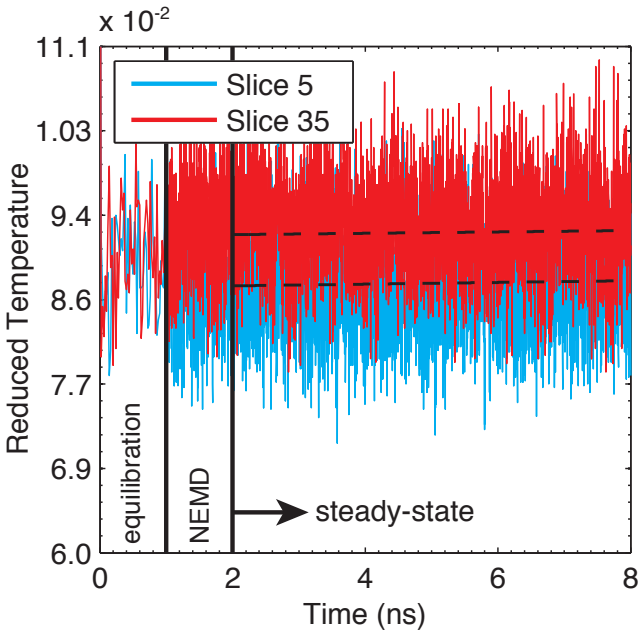

Figure 2. TEMPERATURE OF SELECTED SLICES VERSUS TIME.

spatial-temperature profiles, an effective temperature drop was determined and thermal boundary conductance at the interface between the crystals was calculated via Eq. 1 The thermal conductivities of the crystals themselves were also calculated.

To quantify temperature uncertainty in the steady state regime, a one-sample t-test was performed at an $\alpha = 0.05$ significance level to produce 95% confidence intervals for each time-averaged temperature data point as shown in Figure 3. A sample population consisted of 3000 temperature measurements made via Eq. 5 corresponding to 6 nanoseconds of simulation from the presumed onset of steady-state conditions. The standard deviation of the time-averaged local temperatures was less than 0.6 % of the average values themselves. For the sake of clarity, error bars have therefore been omitted from Fig. 3.

BASELINE THERMAL BOUNDARY CONDUCTANCE

In order to determine the effect of an interstitial layer on h_{BD} at the interface between vibrationally dissimilar LJ crystals, a baseline value must first be known. The baseline thermal boundary conductance value was taken as that at the interface between a LJ crystal with atomic mass equal to 40 amu and an "isotope" LJ crystal with atomic mass equal to 120 amu. This large mismatch in atomic mass results in a large mismatch in vibrational spectrum, as frequencies of atomic vibration are inversely proportional to $m^{1/2}$. Under the elastic scattering approximation, a large vibrational mismatch should result in relatively low thermal transport across the interface, since only those lattice vibrations

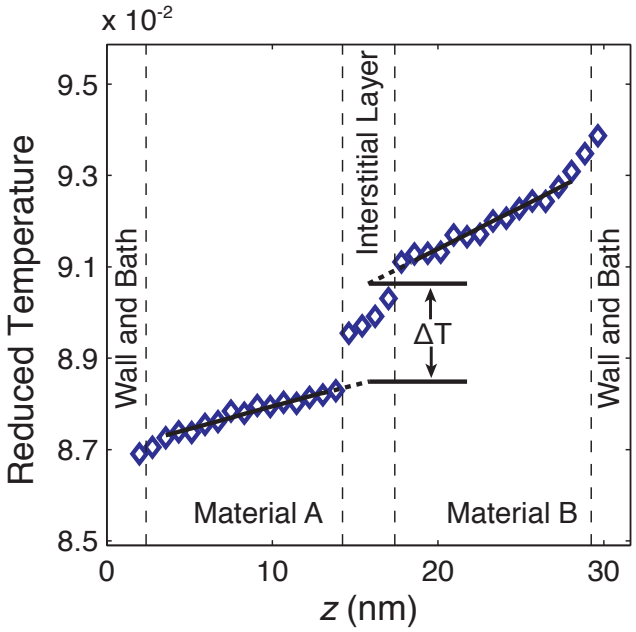

Figure 3. EXAMPLE OF TIME-AVERAGED TEMPERATURE PROFILE.

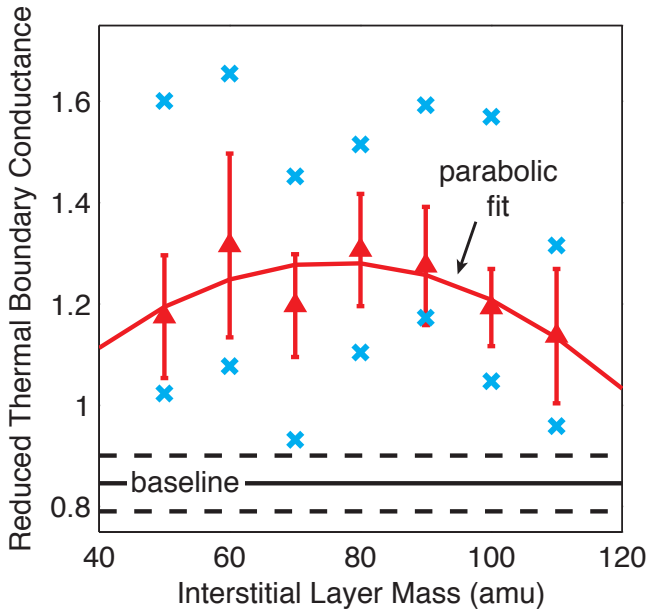

Figure 4. INTERSTITIAL LAYER RESULTS.

that exist at the same frequencies in each material comprising the interface can participate in interfacial transport. Experimental data has also revealed this trend [6].

To explore the sensitivity and repeatability of the baseline results, 10 independent simulations with unique seed values were used. The baseline value of thermal boundary conductance is calculated as the mean of these 10 simulations. The resulting mean baseline value is 0.8456 with a standard deviation of 0.0549.

EFFECT OF AN INTERSTITIAL LAYER

The effect of an interstitial layer was investigated by adding a six unit cell thick layer in the middle of the computational cell, as shown in Fig. 1b. The interatomic interaction in the interstitial layer was the same as in the rest of the system, but the masses of the atoms comprising the layer were systematically assigned values ranging from 50 to 110 amu in 10 amu increments. The calculated values of h_{BD} are shown in Fig. 4 along with the baseline measurements discussed previously. In total, 10 independent simulations were carried out at each interstitial layer mass value. The maximum and minimum h_{BD} values, as indicated by X symbols in Fig. 4, were removed from each data set in order to prevent extreme realizations from skewing the results in light of the relatively small sample size. Each individual triangle represents the mean and standard deviation of the data set consisting of these 8 data points excluding the maximum and minimum values. A second order polynomial curve was fit to the data to further illuminate the trends demonstrated in these results.

The fit demonstrates an inverse parabolic relation between h_{BD} and m, where the greatest h_{BD} value occurs as the mass of the interstitial layer approaches the mean value of the masses corresponding to the two adjacent crystals (80 amu). This study demonstrates that h_{BD} can be increased by nearly 50% at an interface characterized by a large vibrational mismatch through the use of an interstitial layer. The increase in h_{BD} can be attributed to the bridging of vibrational properties in the presence of the interstitial layer where the vibrational spectrum falls between those of the adjacent crystals comprising the interface. As a result of increased vibrational coupling at the interface, phonon scattering is reduced, increasing thermal boundary conductance in each case examined.

CONCLUSION

Methods for tuning and enhancing thermal boundary conductance are increasingly important in the design of nanoscale devices. Using non-equilibrium molecular dynamics, it was shown that an interstitial layer may be used to effectively bridge the vibrational mismatch of materials at an interface, resulting in enhanced vibrational coupling and, thus, enhanced thermal transport. The vibrational properties of a six unit cell thick interstitial layer were controlled by varying the mass of atoms in the layer. Simulation results indicate that thermal boundary conductance can be increased by up to 50% due to the bridging of vibrational spectra in the presence of an interstitial layer.

ACKNOWLEDGMENT

The authors acknowledge the financial support of the Air Force Office of Scientific Research (Grant No. FA9550-09-1-0245) and the Office of Naval Research through a MURI grant (Grant No. N00014-07-1-0723). J.C.D. is greatly appreciative for financial support from the National Science Foundation through the Graduate Research Fellowship Program.

REFERENCES

[1] Chen, G., 2005. *Nanoscale Energy Transport and Conversion: A Parallel Treatment of Electrons, Molecules, Phonons, and Photons*. Oxford University Press.

[2] Cahill, D. G., Ford, W. K., Goodson, K. E., Mahan, G. D., Majumdar, A., Maris, H. J., Merlin, R., and Phillpot, S. R., 2003. "Nanoscale thermal transport". *Journal of Applied Physics,* ***93***(2), pp. 793–818.

[3] Kapitza, P. L., 1941. "The study of heat transfer in helium II". *Soviet Physics JEPT,* ***11***, pp. 1–31.

[4] Stoner, R. J., and Maris, H. J., 1993. "Kapitza conductance and heat flow between solids at temperatures from 50 to 300 K". *Physical Review B,* ***48***(22), pp. 16373–16387.

[5] Lyeo, H.-K., and Cahill, D. G., 2006. "Thermal conductance of interfaces between highly dissimilar materials". *Physical Review B,* ***73***, p. 144301.

[6] Stevens, R. J., Smith, A. N., and Norris, P. M., 2005. "Measurement of thermal boundary conductance of a series of metal-dielectric interfaces by the transient thermoreflectance technique". *Journal of Heat Transfer,* ***127***, pp. 315–322.

[7] Costescu, R. M., Wall, M. A., and Cahill, D. G., 2003. "Thermal conductance of epitaxial interfaces". *Physical Review B,* ***67***, p. 054302.

[8] Hopkins, P. E., Norris, P. M., Stevens, R. J., Beechem, T. E., and Graham, S., 2008. "Influence of interfacial mixing on thermal boundary conductance across a chromium/silicon interface". *Journal of Heat Transfer,* ***130***, p. 062402.

[9] Daly, B. C., Maris, H. J., Imamura, K., and Tamura, S., 2002. "Molecular dynamics calculation of the thermal conductivity of superlattices". *Physical Review B,* ***66***(2), p. 024301.

[10] Termentzidis, K., Chantrenne, P., and Keblinski, P., 2009. "Nonequilibrium molecular dynamics of the in-plane thermal conductivity of superlattices with rough interfaces". *Physical Review B,* ***79***, p. 214307.

[11] Ivanov, D. S., and Zhigilei, L. V., 2003. "Combined atomistic-continuum modeling of short-pulse laser melting and disintegration". *Physical Review B,* ***68***, p. 064114.

[12] Pickett, W. E., Feldman, J. L., and Deppe, J., 1996. "Thermal transport across boundaries in diamond structure materials". *Modelling and Simulation in Materials Science and Engineering,* ***4***, pp. 409–419.

[13] Maiti, A., Mahan, G. D., and Pantelides, S. T., 1997. "Dynamical simulations of nonequilibrium processes - heat flow and the kapitza resistance across grain boundaries". *Solid State Communications,* ***102***(7), pp. 517–521.

[14] Twu, C.-J., and Ho, J.-R., 2003. "Molecular-dynamics study of energy flow and the kapitza conductance across an interface with imperfection formed by two dielectric thin films". *Physical Review B,* ***67***, p. 205422.

[15] Stevens, R. J., Zhigilei, L. V., and Norris, P. M., 2007. "Effects of temperature and disorder on thermal boundary conductance at solid-solid interfaces: nonequilibrium molecular dynamics simulations". *International Journal of Heat and Mass Transfer,* ***50***, pp. 3977–3989.

[16] Lyver IV, J. W., and Blaisten-Barojas, E., 2009. "Effects of the interface between two lennard-jones crystals on the lattice vibrations: a molecular dynamics study". *Journal of Physics: Condensed Matter,* ***21***(34), p. 345402.

[17] Landry, E. S., and McGaughey, A. J. H., 2009. "Thermal boundary resistance predictions from molecular dynamics simulations and theoretical calculations". *Physical Review B,* ***80***(16), p. 165304.

[18] Schelling, P. K., Phillpot, S. R., and Keblinski, P., 2002. "Comparison of atomic-level simulation methods for computing thermal conductivity". *Physical Review B,* ***65***, p. 144306.

[19] Hegedus, P. J., and Abramson, A. R., 2006. "A molecular dynamics study of interfacial thermal transport in heterogeneous systems". *International Journal of Heat and Mass Transfer,* ***49***(25-26), pp. 4921 – 4931.

[20] Matyushov, D. V., and Schmid, R., 1996. "Calculation of Lennard-Jones energies of molecular fluids". *The Journal of Chemical Physics,* ***104***(21), pp. 8627–8638.

[21] Berendsen, H. J. C., Postma, J. P. M., van Gunsteren, W. F., DiNola, A., and Haak, J. R., 1984. "Molecular dynamics with coupling to an external bath". *Journal of Chemical Physics,* ***81***(8), pp. 3684–3690.